Environmental Science
Processes & Impacts

PAPER

Cite this: *Environ. Sci.: Processes Impacts*, 2015, **17**, 775

Nanoscale mapping of carbon oxidation in pyrogenic black carbon from ancient Amazonian anthrosols†

B. S. Archanjo,*[a] D. L. Baptista,[b] L. A. Sena,[a] L. G. Cançado,[ac] N. P. S. Falcão,[d] A. Jorio[c] and C. A. Achete[ae]

Received 5th November 2014
Accepted 5th February 2015

DOI: 10.1039/c4em00590b

rsc.li/process-impacts

Understanding soil organic matter is necessary for the development of soil amendments, which are important for sustaining agriculture in humid tropical climates. Ancient Amazonian anthrosols are uniquely high in black recalcitrant carbon, making them extremely fertile. In this study, we use high-resolution electron microscopy and spectroscopy to resolve the oxidation process of carbon in the nanoscale crystallites within the black carbon grains of this special soil. Most alkali and acid chemical extraction methods are known to cause chemical modifications in soil organic matter and to give poor or no information about the real spatial structure of soil aggregates. However, here we show that carbon–oxygen functional groups such as phenol, carbonyl, and carboxyl dominate over different spatial regions, with areas varying from over tens to hundreds of nm^2. The chemical maps show that in the nanoscale grain, the surface has a tendency to be less aromatic than the grain core, where higher oxidative-degradation levels are indicated by the presence of carbonyl and carboxyl groups. A deep understanding of these structures could allow artificial reproduction of these natural events.

Environmental impact

In this work, we studied carbon nanoparticles found in ancient anthropogenic sites in South America, named Amazonian dark earths. These sites are covered by soils that have held the secret for a sustainable land-use system in the humid tropics, with the generation of a carbon-negative industry. It is known that the key aspect behind the high productivity and recalcitrance of these soils is the presence of millenary stable carbon structures. There are efforts to reproduce these highly fertile soils by adding charcoal as a soil conditioner. The structural aspects revealed here may be the key for an important improvement in world agriculture and ecosystem sustainability.

Introduction

Highly fertile anthropogenic Amazonian soils, called *Terra Preta de Índio* (TPI) or Amazonian dark earth, exhibit higher concentrations of biomass-derived black carbon (biochar) than adjacent soils.[1–4] Some research has shown that the high levels of black carbon materials in this soil are responsible for its high fertility over long-term cultivation.[1–6] Because of this, several strategies have aimed to develop a charcoal soil amendment based on TPI soils.[2,6,7] Some groups have proposed the production of *terra preta nova* (new Amazonian dark earth or synthetic *terra preta*), with the addition of charcoal and organic biowaste as a soil conditioner. These additives could improve the cation-exchange capacity, stability, and recalcitrance of the soil.[5–10] Nevertheless, the complex carbon-grain structure of TPI soils and the aging effects on its poly-condensed aromatic structure over thousands of years greatly affect the efficacy of biochar as a soil amendment. Previous studies have shown that aged biochar exhibited changes in surface chemistry and adsorption properties,[3,5,6,11] which probably led to high cation retention, as in the Amazonian dark earths.

We have recently used tools for materials science to demonstrate that the millenary black carbons in Amazonian dark earths (TPI-carbon) exhibit a complex morphology, with particles ranging in size from microns to nanometres. Nanocrystallite sizes of sp^2 ordered carbons have been observed in the range of a few to tens of nanometres,[12] changing from the core to the surface of the

[a]*Instituto Nacional de Metrologia, Qualidade e Tecnologia, Av. Nossa Senhora das Graças, 50, 25250-020 Duque de Caxias, RJ, Brazil. E-mail: bsarchanjo@inmetro.gov.br*

[b]*Instituto de Física, PPGMicro, Universidade Federal do Rio Grande do Sul, Porto Alegre, RS, 91501-970, Brazil*

[c]*Departamento de Física, ICEx, Universidade Federal de Minas Gerais, Belo Horizonte, MG 30123-970, Brazil*

[d]*Departamento de Ciências Agronômicas, Instituto Nacional de Pesquisas da Amazônia, Manaus, AM 69011-970, Brazil*

[e]*Departamento de Engenharia Metalúrgica e de Materiais, Universidade Federal do Rio de Janeiro, Cx. Postal 68505, Rio de Janeiro, RJ 21945-970, Brazil*

† Electronic supplementary information (ESI) available. See DOI: 10.1039/c4em00590b

TPI-carbon grains.[13] Also, one can find studies where nanotechnology tools are used in soil science research.[14,15] In the present work, we use state-of-the-art nanotechnology tools to gain an understanding of the TPI-carbon structures. Scanning electron microscopy (SEM) coupled with an energy dispersive X-ray (EDX) detector was first used to identify and map the chemical elements of the TPI-carbon grain in the microscale range. In sequence, thin lamellae were prepared using a focused ion beam (FIB) for transmission electron microscopy (TEM) analysis. Nanometre-scale chemical bonding maps (a spatial resolution of 10 nm and an energy resolution of approximately 0.16 eV) of TPI-carbon grains were then obtained through the spectral imaging technique in electron energy loss spectroscopy (EELS) experiments associated with scanning transmission electron microscopy (STEM). Nanoscale spatial-resolved maps of carbon electronic transitions were built to spatially resolve the chemical structure of organic radicals across the TPI-carbon grains (TPI grains rich in carbon). For comparison, EELS experiments were performed on different charcoal samples produced in the laboratory.

Experimental

The TPI samples were collected near Manaus, Amazonas State, Brazil, from three sites: Serra Baixa – TPI_{SB} – (Costa do Açutuba), Iranduba (Lat. 3° 30′ S, Long. 60° 20′ W), Balbina – TPI_{BB} – Presidente Figueiredo (Lat. 1° 54′ S, Long. 59° 28′ W) and Costa do Laranjal – TPI_{CL} – and Manacapuru (Lat. 3° 18′ S, Long. 60° 33′ W). The samples were extracted from the surface layer (0–20 cm depth) using a Dutch auger. The charcoal sample was produced at *Instituto Nacional de Pesquisa da Amazonia* (INPA) using Ingá wood (*Ingá edulis* Mart.), a typical Amazonian plant species. The branches of Ingá from a 7 year old tree were placed in a pyrolysis furnace. The 600 °C (ref. 16) combustion temperature was accomplished in a pyrolysis furnace of refractory brick with 20 L capacity, reaching the temperature after 2 h. Afterwards, the furnace was turned off and allowed to cool. Finally, the samples were filtered in a 2 mm sieve. Detailed spectroscopic analyses and soil science data from these samples can be found elsewhere.[12,13,17]

SEM, microscale energy dispersive X-ray spectroscopy (EDX), and *in situ*-lift-out and thinning processes for the TEM sample preparation were carried out using a Nova NanoLab™ 600 DualBeam platform (SEM and FIB) from FEI Company. TEM, STEM, and spatially localized EELS analyses were performed on a Cs-corrected Titan 80-300 transmission electron microscope (FEI Company), equipped with a Gatan Tridiem Imaging Filter. The EELS spectra were collected using an electron monochromator, reaching an ultimate energy resolution of 0.16 eV, and the EELS analysis was performed in STEM mode, allowing sub-nanometre-scale spatial resolution. Spectrum-imaging data (EELS spectrum collected at each pixel) were recorded for EELS during a drift-corrected STEM experiment.

Results and discussion

Before developing the spatially resolved chemical analysis, we structurally characterized our TPI-carbon material at the microscopic scale. Fig. 1 shows typical SEM images of arbitrarily collected TPI grains and a charcoal grain measured on a scale of tens of micrometres. The grains, which are typically nonspherical, presented random shapes and forms.

The chemical composition performed using EDX of hundreds of grains revealed that, in addition to C, Si, and O, which are common to all grains, elements such as Al, Fe, Cl, Ca, Mg, P, K Ti, Na, Mn, Ti, and Zr may be present (for more information about the chemical elements found in the grains in Fig. 1, see Fig. S1–S4 in the ESI†). Both shape and chemical composition were in agreement with the natural TPI origin, which is based on the mineral soil organic matter aggregation.[3,8,18–20] Comparing the TPI_{SB}-carbon grain in Fig. 1e with the charcoal grain in Fig. 1f, a very similar microstructure can be seen, as the plant stalk vessels are visible in both images. The dispersion of TPI grains with high C concentration detected in all the TPIs analysed in this study confirms that aged charcoal is the main source of biochar or black carbon in TPI soils, in agreement with previous studies.[3,12,13,20–23]

To gain a better understanding of the distribution of chemical elements in the TPI-carbons, several black grains were selected using optical microscopy and SEM, and divided into two parts using a scalpel. The first important observed characteristic common to all black grains was a compact carbon core structure surrounded by a porous shell layer, where mineral aggregates are present. In an optical image contrast, the core was found to have a graphite-black colour, while the shell had a brighter contrast or a grey colour (Fig. 2a). A SEM image taken roughly from the same region as in Fig. 2a is shown in Fig. 2b. The EDX spectrum averaged over the total area is plotted in Fig. 2c, where the presence of C, O, Al, Si, and, in lower amounts, Fe, P, and Ca, was all clearly detected. The spatial elemental composition of this grain is shown in Fig. 2d–k, which illustrates EDX intensity maps for different chemical elements (indicated in the upper-right side of each image). The main observations are (i) the basic composition of the core is C;

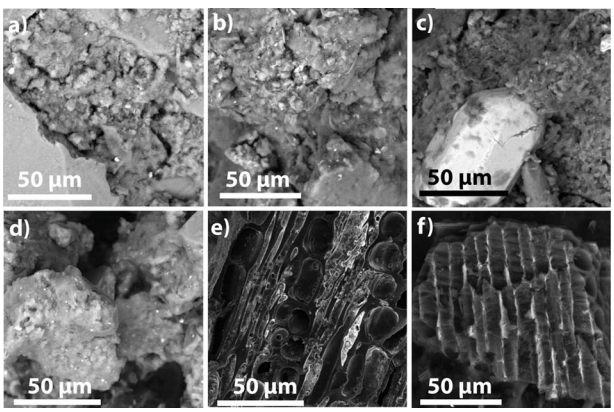

Fig. 1 SEM images of arbitrarily selected grains of TPI obtained from different sites, and charcoal. (a) Grains taken from Balbina – TPI_{BB} – Presidente Figueiredo; (b) Costa do Laranjal – TPI_{CL} – Manacapuru; (c and d) Serra Baixa – TPI_{SB} – Costa do Açutuba; and (e) TPI_{SB}-carbon grain selected from TPI_{SB}. (f) A charcoal grain produced from the Ingá plant. For chemical information, see Fig. S1–S4 in the ESI.†

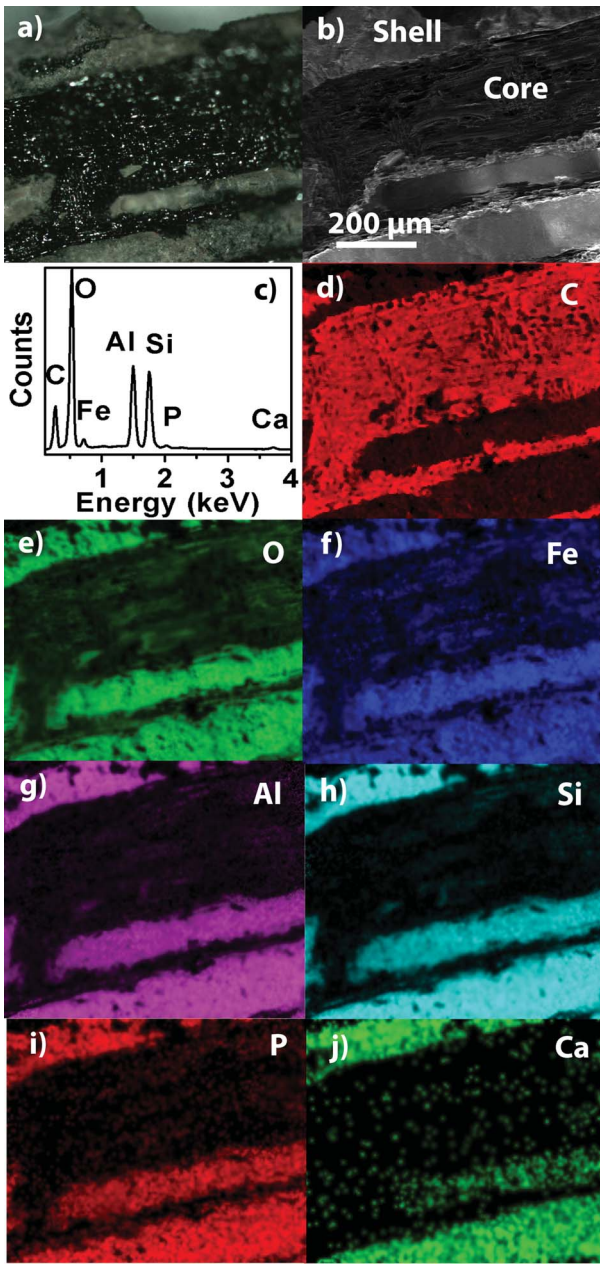

Fig. 2 Microscale analyses of a TPI-carbon grain. (a) Optical image of a TPI-carbon grain and (b) SEM image of the same grain in the same region shown in (a). The core and shell regions are specified in the image. (c) EDX spectrum collected in the whole image shown in (b). From (d) to (j), EDX maps from the different chemical elements present in this TPI-carbon grain. The elements are labelled on the top-right of each figure.

(ii) O is spread over the whole structure; and (iii) Fe, Al, Si, Ca, and P are mainly located in the shell.

Next, TEM, STEM, and EELS measurements were performed. The core–shell interfaces were cut using an FIB setup operated at a dual beam platform using a Ga^+ ion source working at 30 keV accelerating energy. Thin cross-sections were removed and welded onto a lift-out copper grid for subsequent analyses. Unlike other studies,[3,19] during the TEM sample preparation method used here, no embedding medium was needed to section and stabilize the thin TEM lamella. Chemical mappings were post-constructed by selecting data from specific energy regions from the EELS spectrum dataset. STEM images were acquired using a high-angle annular dark-field (HAADF) detector.

Fig. 3 links the microscopic analyses displayed in Fig. 1 and 2 with the nanoscopic analysis, which was further developed to achieve the spatially resolved chemical analysis within a few nanometres resolution. This procedure was applied to TPI-carbon grains selected from different TPI sites which are hundreds of kilometres apart from each other. All grains analysed here showed a similar spatial distribution of the chemical elements and organic radicals in both micro- and nanoscale.

The STEM analyses of the TPI-carbon cross-sectioned slices showed two topologically distinct zones (Fig. 3b). One zone demonstrated a continuous contrast (microns in scale) and composes the bulk of the grain core. The other zone, which was located on the external surface of the grain, composes the shell. This region exhibited a nanometre-scale porous structure and is formed by aggregates of assembled 10–1000 nm particles. This result is in agreement with a previous analysis by Jorio *et al.*[12] A TEM image of a typical nanometre carbon particle extracted from the external region of the TPI-carbon grain is shown in Fig. 3c. The particle surface is formed by smaller structures, which are several tens-to-hundreds of nanometres in length.

The energy-loss regions investigated by EELS covered the C ionization K-edge around 285 eV. Chemical bonding maps were constructed from the energy loss near-edge fine structure (ELNES) of the carbon K-edge. This fine structure represents the transition from the C 1s electronic core state to the unoccupied valence states (π^*) above the Fermi level. Typical EELS spectra from the TPI-carbon shell and core (Fig. 3b) are displayed in Fig. 4a (upper and middle spectra, respectively). We also show the EELS spectra of the charcoal sample for comparison (bottom spectrum in Fig. 4a). The similarity between the TPI-carbon core and the charcoal is evident, while the TPI-carbon surface spectrum shows different relative peak intensities.

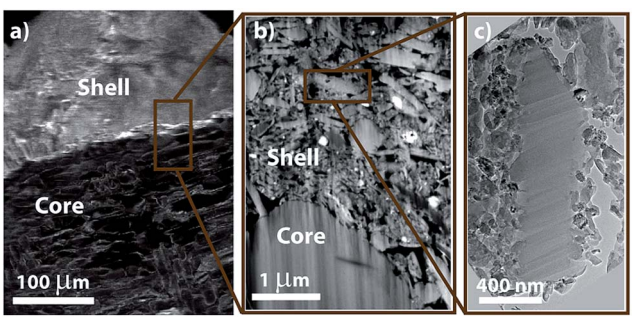

Fig. 3 Electron microscopy images from microscopic to nanoscopic analysis. (a) Higher magnification of the SEM image shown in Fig. 2b, highlighting a specific area where detailed chemical analysis will be performed after FIB preparation. (b) HAADF-STEM image of a thin lamella showing the interface between the graphitic core and its porous nano-structured surface (shell). (c) TEM image of a single carbon nanoparticle on the porous nano-structured surface.

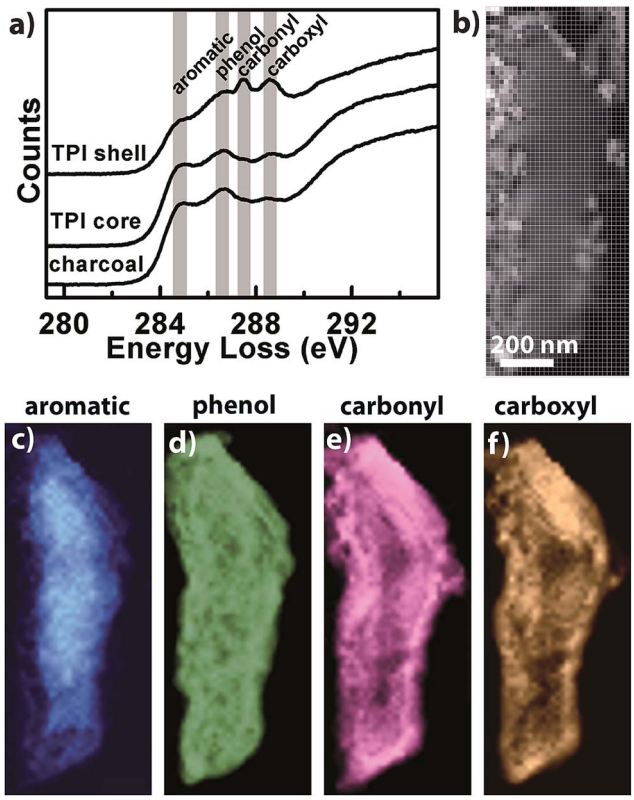

Fig. 4 Chemical bonding information of a TPI-carbon grain (the same as shown in Fig. 3c) and charcoal. (a) EELS spectra from charcoal used in this work (bottom), the core of the TPI-carbon grain (middle), and from the TPI-carbon-grain shell (bottom). The grey stripes define the energy range where energy selective maps [shown in panels (c–f)] were obtained. (b) Grid representing the spatial resolution of our EELS system. From (c) up to (f), filtered EELS images showing chemical bonding maps of the organic radicals (aromatic, phenol, carbonyl, and carboxyl). See Fig. S5 and S6 in the ESI† for additional details on the nanoscale chemical bonding information of TPI-carbon grains originated from different TPI sites.

Besides the carbon 1s → σ* broadband above 290 eV, four well-defined peaks are evident in the range of the electronic transition 1s → π*.[24] Observing the EELS spectra shown in Fig. 4a, we assigned them to the aromatic carbon (C sp^2) peak around 285, the phenol (C–OH) at 286.7, the carbonyl (C=O) at 287 eV, and the carboxyl group (HO=C–O) at 288.6 eV.[11,12,19,22,25] Spatially resolved mapping of each functional group is presented in Fig. 4c–f. The spatially resolved measurement grid is shown in Fig. 4b, where the experimental points are spaced 15 nm apart. The chemical maps show that the grain core has a tendency to be more aromatic (graphitic) than the grain surface. In addition, the results clearly show that the aging-induced oxidation is not homogeneous in the sample within the spatial resolution of 15 nm, revealing chemical domains ranging from tens to hundreds of nm^2. Higher oxidative-degradation levels indicated by the presence of carbonyl and carboxyl groups were more pronounced on the grain surface. These results are consistent with the work reported by Liang *et al.*[11] However, our analysis goes further, showing local variations (in the range of a few nanometres) on the main organic radicals, consistent with previous observations of nanocrystallites composed of sp^2 carbon.[12,13]

Carboxylic groups at the surface of the grain increase the cation exchange capacity in the soil, retaining nutrients and driving the fertility level of the soil.[3,6] Hence, the inner aromatic regions act as a source of carbon to keep the oxidization process of the grains over the years. The core of the microscale grain shown in Fig. 2 remains more aromatic than the nucleus of the smaller particle shown in Fig. 4, even after thousands of years. It is worth noticing that the spectral characteristics of the core of the TPI-carbon micrograins are similar to those of fresh charcoal, presenting low levels of oxidation and low amounts of carbonyl and carboxyl groups.

Although the results presented here about the nano-structure of the carbon present in the TPI can be useful to predict change trajectories in "modern" charcoal when added to the soil, a considerable effort still has to be made before we have a recipe to reproduce these structures in the laboratory. For example, there are many questions related to the availability of the anions and cations found on the shell of the nanoscale TPI-carbon grain. In previous studies,[12,13,17] we have shown that the stability of calcium attached to a nanoscale oxidized carbon grain strongly depends on the size and functional organic groups of the latter. Although calcium has been chosen as a prototype for these studies, additional work is necessary for understanding the relationship between the size of the nanoscale carbon structures found in the TPIs, and the stability of the ions hosted by them. In a next stage, questions related to the organic groups and chemical elements interacting with carbon grains at nanoscale should be answered, giving rise to important ingredients to reproduce TPI properties in feasible scale, time, and cost for technological applications.

Conclusions

We presented a spatially resolved chemical nanoscale analysis of the black carbon found in Amazonian dark earths. It is possible that the carbon phase in TPI begins as a charcoal-like carbon structure of mostly poly-condensed aromatic groups. This structure provides a prolonged biological and chemical stability. However, slow partial oxidation and/or aggregation of organic molecules present in soil organic matter over thousands of years produce oxidized carbon at the surface. This surface carbon is not fully homogeneous at the nanoscale, where different oxidized carbon functional groups, such as phenol, carbonyl, and carboxyl, dominate the spectra in the range of tens of nanometres in different areas.

To date, scientists have been unable to fully reproduce the beneficial growth properties of TPI. It is hypothesized that, to achieve these benefits, the black carbon or biochar must be aged to promote oxidization, thus increasing the cation-exchange capacity of the soil. Therefore, fresh charcoal must be altered before it can function as a biotope. The inhomogeneous distribution of the different functional groups at the tens-of-nanometre scale indicates that it may be feasible to establish a non-simultaneous oxidation process that favours different oxidized carbon functional groups at the same time.

Acknowledgements

This work was financed by Inmetro, FAPERJ, INPA, FAPEAM and CNPq, including the *Rede Nacional de Pesquisa e Instrumentação em Nano Espectroscopia Óptica*. L.G.C. acknowledges the Brazilian agencies FAPEMIG and CNPq. A.J. acknowledges financial grant support from PRONEX-BioNC, FAPEMIG, and CNPq (473840/2012-0 Universal grant). B.S.A. acknowledges J. R. Araujo for fruitful discussions and also L. R. Lidízio, C. A. Senna, and A. M. Pimenta for their help with the EDX experiments.

Notes and references

1 A. Briones, *Front. Microbiol.*, 2012, **3**, 1–6.
2 B. Glaser, L. Haumaier, G. Guggenberger and W. Zech, *Naturwissenschaften*, 2001, **88**, 37–41.
3 B. Liang, J. Lehmann, D. Solomon, J. Kinyangi, J. Grossman, B. O'Neill, J. O. Skjemstad, J. Thies, F. J. Luizão, J. Petersen and E. G. Neves, *Soil Sci. Soc. Am. J.*, 2006, **70**, 1719–1730.
4 E. Marris, *Nature*, 2006, **442**, 624–626.
5 C.-H. Cheng and J. Lehmann, *Chemosphere*, 2009, **75**, 1021–1027.
6 E. H. Novotny, M. H. B. Hayes, B. E. Madari, T. J. Bonagamba, E. R. deAzevedo, A. A. de Souza, G. X. Song, C. M. Nogueira and A. S. Mangrich, *J. Braz. Chem. Soc.*, 2009, **20**, 1003–1010.
7 J. Lehmann, *Nature*, 2007, **447**, 143–144.
8 C. H. Chia, P. Munroe, S. Joseph and Y. Lin, *Soil Res.*, 2010, **48**, 593–605.
9 B. Glaser, *Philos. Trans. R. Soc., B*, 2007, **362**, 187–196.
10 B. Glaser, J. Lehmann and W. Zech, *Biol. Fertil. Soils*, 2002, **35**, 219–230.
11 B. Liang, C. Wang, D. Solomon, J. Kinyangi, F. J. Luizão, S. Wirick, J. O. Skjemstad and J. Lehmann, *Br. J. Environ. Clim. Change*, 2013, **3**, 15.
12 A. Jorio, J. Ribeiro-Soares, L. G. Cançado, N. P. S. Falcão, H. F. Dos Santos, D. L. Baptista, E. H. M. Ferreira, B. S. Archanjo and C. A. Achete, *Soil Tillage Res.*, 2012, **122**, 61–66.
13 J. Ribeiro-Soares, L. G. Cançado, N. P. S. Falcão, E. H. Martins Ferreira, C. A. Achete and A. Jorio, *J. Raman Spectrosc.*, 2013, **44**, 283–289.
14 M. Baalousha, M. Motelica-Heino, S. Galaup and P. Le Coustumer, *Microsc. Res. Tech.*, 2005, **66**, 299–306.
15 M. A. Wilson, N. H. Tran, A. S. Milev, G. S. K. Kannangara, H. Volk and G. Q. M. Lu, *Geoderma*, 2008, **146**, 291–302.
16 A. Mukherjee, A. R. Zimmerman and W. Harris, *Geoderma*, 2011, **163**, 247–255.
17 B. S. Archanjo, J. R. Araujo, A. M. Silva, R. B. Capaz, N. P. Falcão, A. Jorio and C. A. Achete, *Environ. Sci. Technol.*, 2014, **48**, 7445–7452.
18 C. H. Chia, P. Munroe, S. D. Joseph, Y. Lin, J. Lehmann, D. A. Muller, H. L. Xin and E. Neves, *J. Microsc.*, 2012, **245**, 129–139.
19 J. Lehmann, B. Liang, D. Solomon, M. Lerotic, F. Luizão, J. Kinyangi, T. Schäfer, S. Wirick and C. Jacobsen, *Global Biogeochem. Cycles*, 2005, **19**, GB1013.
20 B. Glaser, E. Balashov, L. Haumaier, G. Guggenberger and W. Zech, *Org. Geochem.*, 2000, **31**, 669–678.
21 I. Cohen-Ofri, R. Popovitz-Biro and S. Weiner, *Chem.–Eur. J.*, 2007, **13**, 2306–2310.
22 J. Lehmann, S. Dawit, K. James, D. Lena, W. Sue and J. Chris, *Nat. Geosci.*, 2008, **1**, 238–242.
23 M. W. I. Schmidt, J. O. Skjemstad and C. Jäger, *Global Biogeochem. Cycles*, 2002, **16**, 1123.
24 P. K. Chu and L. H. Li, *Mater. Chem. Phys.*, 2006, **96**, 253–277.
25 C. M. Chen, J. J. Dynes, J. Wang, C. Karunakaran and D. L. Sparks, *Environ. Sci. Technol.*, 2014, **48**, 6678–6686.